# REFLECTIVITY WAVEFIELD INVERSION OF SYNTHETIC DATA FROM ELASTIC AND VISCOELASTIC ANISOTROPIC FLAT-LAYERED, SHALE-BOUNDED, FRACTURED SANDSTONE RESERVOIR MODELS

SYLVIA PACHECO and GEORGE A. MCMECHAN

*Center for Lithospheric Studies, The University of Texas at Dallas, 800 W. Campbell Road, Richardson, TX 75080-3021, U.S.A. mcmec@utdallas.edu*

(Received December 23, 2012; revised version accepted May 2, 2013)

ABSTRACT

Pacheco, S. and McMechan, G.A., 2013. Reflectivity wavefield inversion of synthetic data from elastic and viscoelastic anisotropic flat-layered, shale-bounded fractured sandstone reservoir models. *Journal of Seismic Exploration*, 22: 223-250.

Full-wavefield inversion based on frequency-domain reflectivity modeling is developed and applied, in the $\tau$-p domain, to synthetic data for flat-layered viscoelastic, anisotropic models. P- and S-wave quality factors and HTI and VTI anisotropy are extracted, by inversion, from synthetic data for viscoelastic, fractured sand reservoir models. Ignoring viscoelasticity or anisotropy results in errors and increased uncertainty in the estimates of the other seismic parameters, as the parameterization is incomplete. Increasing the number of layers or parameters, or adding noise, makes the inversion more difficult to converge to the correct solution; parameter correlations confirm this observation, showing more inter-layer correlations. The noise is mainly left in the residual wavefield. Better results are obtained with layer stripping than without, as the solution space has fewer local minima when the model contains fewer parameters (fewer degrees of freedom). Multiple layer stripping runs, solving for parameters adjacent pairs of layers together, improves the inversion performance and the accuracy of the results.

KEY WORDS: wavefield seismic inversion, sandstones, reflectivity, $\tau$-p, viscoelastic, anisotropic

0963-0651/13/$5.00 

## INTRODUCTION

A productive strategy in algorithm development is to move from simple to more complicated, complete and realistic parametrizations, with corresponding progressive advances in capability and understanding. For example, gradually adding more parameters to seismic inversion provides more information from the seismic data, to investigate the interactions between parameters, and to allow inclusion of constraints from petrophysical parameters measured at well locations. Previous studies separately compare seismic responses of scalar, acoustic, elastic, viscoelastic or anisotropic media (Ozdenvar and McMechan, 1997; Koesoemadinata and McMechan, 2003; Tiwari and McMechan, 2007a; Chang and McMechan, 2009a,b; Hu and McMechan, 2010). As more parameters are added to an inversion, it becomes more difficult to invert for them because of the limited information content associated with limited offset and angular apertures, frequency, recorded components, error accumulation, and so forth. However, as shown below, many of these can be significantly mitigated by a layer stripping-approach which reduces the number of parameters to be solved simultaneously.

Previous inversions for 1D acoustic and elastic media are shown by McCaulay (1986), Pan et al. (1988), and Pica et al. (1990). Stoffa and Sen (1992) used covariance matrices to investigate the relations between inverted elastic properties and showed the importance of maintaining high frequency bandwidth and large angle apertures, and of constraining the posterior probability density functions.

The reflectivity modeling approach used below is defined only for flat layered media but is very fast (as it is an analytic solution), and complete (in that it includes all internal multiples and converted waves); thus, with this approach it is possible to do, not only numerical synthesis of seismograms for specific reservoir configurations, but also full-wavefield inversions for parameters of composite viscoelastic, anisotropic (VTI or HTI) layers. Below, we illustrate and evaluate this capability, using synthetic data.

Characterizing fracture patterns is important for improved understanding of fluid flow, and anisotropy is related to the presence of fractures (e.g., Maultzsch et al., 2003). Anisotropy is most evident in changes of velocity as a function of direction. In the synthetic examples below, we use models of fractured sandstone reservoirs, and estimate the anisotropy by full-wave inversion of synthetic elastic seismic data. Fractured sandstone reservoirs occur worldwide. The structure of a few fractured sandstone reservoirs have been evaluated to predict fluid flow. Petrographic studies of fractured reservoirs (Kelly et al., 2000) allow characterization of hydrocarbon fluid migration in sandstones of Carboniferous age in the Ouachita Mountains in Oklahoma, and in the Jurassic East Berlin Formation in the Hartford Basin, Connecticut. For

the Mesaverde Group, San Juan basin, New Mexico, scanning electron microscope data show that fracture orientation often remains constant through different scales (Ortega and Marrett, 2000). 3D modeling of a fracture network in Emsian sandstone outcrops in the Moroccan Anti-Atlas, shows that each fracture obeys the Mohr-Coulomb criterion (Guiton et al., 2003) which improves fracture network modeling for hydrocarbon fields. Fluid flow in fractured rocks depends on the relations between the fracture system and the rock matrix (Maultzsch et al., 2003). The nature of layering also controls the fracture system geometry and scaling, and thus influences the fluid flow; Odling et al. (1999) studied this in different fractured hydrocarbon reservoirs (sandstones, chalk and limestones) around the world. In laboratory studies of fractured sandstone cores from the Southwest German Trias, Baraka-Lokmane (2002) found that gas-based measurements provide a more accurate intrinsic permeability than liquid-based for clay-rich sandstones. Another study of fractured sandstones reservoirs by Hennings et al. (2000) uses a combination of outcrop data and three-dimensional structural models to characterize a fractured sandstone reservoir in Oil Mountain, an asymmetric anticline on the western flank of the Casper arch in central Wyoming.

What is missing in most of the papers listed above is the connection between the fracture properties and their seismic expression, through the rock anisotropy, and vice versa. Previous inversion studies have included Q and anisotropy separately, but not simultaneously. Thus, the goal of this study is to investigate the possibility to invert for viscoelastic and anisotropic parameters in simple layered models of fractured sandstones. Martínez and McMechan (1991a,b) developed reflectivity-based software for full-wavefield modeling and inversion for flat-layered viscoelastic models in the $\tau$-p domain, and used it to invert a Gulf of Mexico field data set. Martínez (1993) evaluates the differences, on AVO, of acoustic, elastic, and viscoelastic modeling. Tiwari and McMechan (2007b) applied the viscoelastic version to show the seismic consequences of changes of fluid content and its spatial distribution with time. Tiwari (2007, personal communication) expanded it to include VTI and HTI anisotropy, but did not apply it to reservoir models. The present study uses this same software, with the addition of both P- and S-wave anisotropy, to illustrate that the information content in synthetic data from viscoelastic anisotropic (elliptical VTI or HTI) media is sufficient to invert simultaneously for the viscoelastic and anisotropic parameters, and an efficient layer-stripping inversion strategy.

The potential of reflectivity-based inversion to define the VTI and HTI anisotropy of targets from data from numerical models of layered sandstone reservoirs is illustrated. Ignoring anisotropy in data from an anisotropic model results in increased uncertainty in the estimates of the other seismic parameters, because reflection times and amplitudes change with anisotropy. These changes are the motivation to include anisotropy as a parameter in viscoelastic reflectivity inversion (Fig. 1).

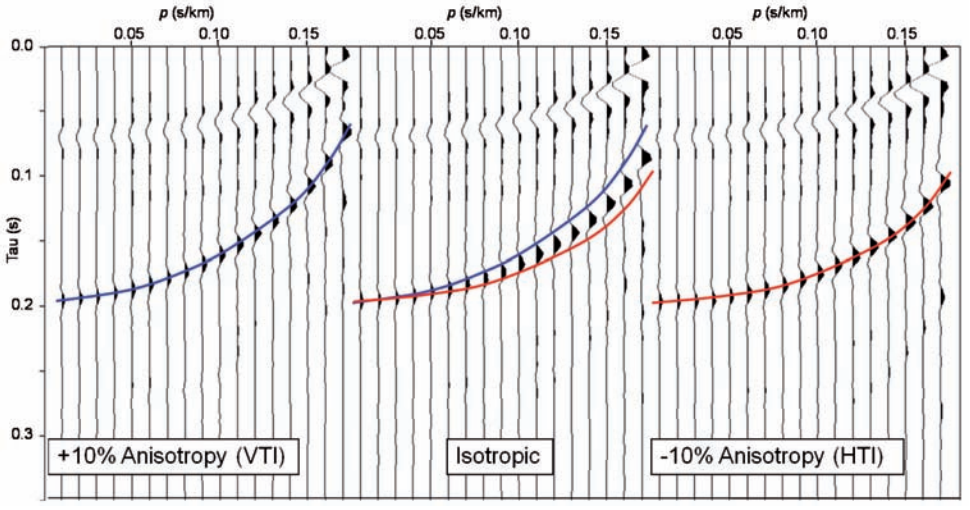


Fig. 1. Changes in amplitudes and times associated with anisotropy. p is slowness; tau ($\tau$) is intercept time.

## METHODOLOGY

Full-wavefield inversion for viscoelastic parameters from $\tau$-p seismic data has been previously implemented using reflectivity to compute the response of flat-layered viscoelastic models (Martínez and McMechan, 1991b; Tiwari and McMechan, 2007a). Inversion is performed using Conjugate Gradient (CG) and Singular Value Decomposition (SVD) methods. CG is a local optimization method that minimizes wavefield residuals by searching for a local minimum. The CG method has the advantages that it is fast for solution of systems of linear equation; it is effective to locate the minimum, and requires a small memory space. SVD provides auxiliary information on resolution, uniqueness and model covariance, but it is slower. To ensure that the auxiliary information is relevant to the final solution, we use SVD only for a single final iteration after convergence of the CG.

### Starting model

The requirement for the starting model for inversion is that it needs to satisfy the half period condition from the target model (Mora, 1989); if it doesn't, convergence may be to a local minimum. This can be implemented by

obtaining an isotropic starting model from conventional moveout analysis (which assumes that the anisotropy is small), and applying a filter that starts from the lowest frequencies and gradually admits higher frequencies as iterations proceed (Pica et al., 1990; Xu et al., 1995) so the half period condition is satisfied for each frequency in turn. Note also, when layer stripping is done, that the half period criterion needs to be satisfied only for each layer as it is added to the solution.

## Elliptic anisotropy

Transverse Isotropy (TI) for P and SV is incorporated as a vertical/horizontal velocity factor PR. The P and SV phase velocities at other propagation angles are approximated by elliptical interpolation between the vertical and horizontal velocities. Thus, for P-waves, PR = 1 is isotropy, PR$<1$ is HTI and PR$>1$ is VTI. For weak anisotropy, and small propagation angles $\theta$ from the VTI axis, the relation between PR and the usual P-wave anisotropy parameter $\delta$ is PR $\sin\theta \approx (1 + \delta\sin^2\theta - \cos\theta)$. See Thomsen (1986, 1992), for a discussion of elliptic anisotropy and it's limitations.

Although the elliptic model (e.g., Bakker, 1995) is often considered to be inadequate for description of anisotropy (e.g., Thomsen, 2002), and inversions for $\delta$, $\varepsilon$ and $\gamma$ from traveltime moveout data alone are nonunique (Barbosa et al., 2008; Grechka, 2009; Bakulin et al., 2010), it has utility when the data lie within a sufficiently small angular aperture around the TI symmetry axis (in which case $\delta$ is the only salient P-wave anisotropy parameter; $\varepsilon$ influences the moveout only at larger angles) (Thomsen, 1986). See Kleyn (1956) and Ohlsen and Macbeth (1999) for field data examples for which the elliptic assumption appears to give a good fit; the latter show 12 North Sea data for which the P-wave errors incurred by assuming elliptical anisotropy are $< 2\%$ for propagation angles up to 60° from the symmetry axis. Recent studies of the properties of elliptic models include Bakulin et al. (2010) and Golikov and Stovas (2012). It is also known that the nonuniqueness inherent in anisotropic traveltime inversions can be resolved when amplitudes are added as data in the inversion (e.g., Chang and McMechan, 2009a) provided that the corresponding model parameterization is also used, The calculations below use amplitudes and are all for propagation angles $\ll 60°$.

## Generation of test data

The petrophysical properties for the host isotropic unfractured sand are porosity $\phi = 22\%$, clay content $= 5\%$ and the natural log of the fluid permeability $\ln\kappa = 6.61$ md. Synthetic seismic data for the examples were obtained from models constructed using the empirical petrophysical-to-seismic

relations for sands of Koesoemadinata and McMechan (2001). The viscoelastic parameters for the test model used (see the Tables below) are the same as those used by Tiwari and McMechan (2007a).

For synthetic trace generation, the source has a band limited (5 to 85 Hz) zero phase wavelet with a dominant frequency of 40 Hz. The synthetic viscoelastic, anisotropic data contain all transmission and conversion effects and internal multiples, but no free surface multiples, as they are computed with no free surface. The source and receivers are located at the bottom of an upper half space, for the modeling and all the inversions. $\tau$-p seismic traces are calculated using the reflectivity algorithm described by Martínez and McMechan (1991a), with the addition of anisotropy. The seismic traces are responses to a point source in a flat-layered model. Trace amplitudes are the total displacement at the geophones and not a component of it (Martínez and McMechan, 1991a; Tiwari and McMechan, 2007a).

We use the petrophysical-to-seismic formulation of Koesoemadinata and McMechan (2001, 2003) to define the appropriate viscoelastic, anisotropic models for generating the test data, the (frequency-domain) reflectivity formulation of Martínez and McMechan (1999a) [based on Kind (1976) and Silva (1976)], for the forward modeling, and of Martinez and McMechan (1999b) [based on damped least squares (Marquardt, 1963)], with adaptive damping factors, for the inversion. The modeling uses Futterman's (1962) dispersion model and complex velocities for the viscoelasticity. Matching of the observed and calculated data is done in the slowness - intercept time (p-$\tau$) domain to eliminate the need for inverse slant stacking at every iteration in the inversion.

## Inversion

After selecting a sequence of flat layered models of shales, and 90% gas saturated sands (gas saturation is $1 - S_w$ , where $S_w$ is water saturation) (Fig. 2), the synthetic common-source $\tau$-p gathers are generated, and full-wavefield inversions are performed until convergence, first with CG and, at the last iteration, with SVD with damping. All PP and PS reflections in the wavefield are fitted to estimate the parameters for each layer (Tiwari and McMechan, 2007a). Convergence is defined by the flattening of the residual amplitude curve. The model parameters estimated by the inversion are compared with those of the known target model for investigation of the inversion behavior for all the seismic parameters including anisotropy, P-wave and S-wave quality factors (for viscoelastic models) and layer thicknesses.

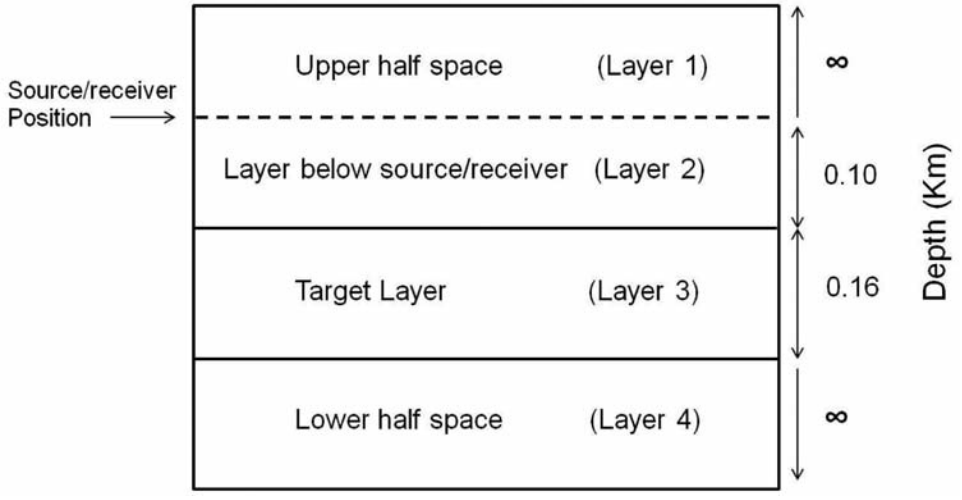


Fig. 2. Model configuration. Dashed line is location of the source and receivers. All layers, except the target layer 3 are shales with Vpo = 2.825 km/s, Vso = 1.202 km/s, $\rho$ = 2.275 g/cm3 , and anisotropy factor = 1.030. The model is homogeneous in the direction perpendicular to the plane, and the vertical fractures in the (HTI) target layers are also oriented perpendicular to this plane (with the horizontal symmetry axis).

Data for different models with up to three targets layers are inverted to solve for the parameters of the target layers. For comparison of the viscoelastic anisotropic results, inversions are first performed for both elastic isotropic and elastic anisotropic models. Anisotropy percentages in HTI and VTI layers are between 5% and 10%. Anisotropic and isotropic inversions are performed to observe differences in results when anisotropy is, and is not, taken into account. The main sequence of examples is for 3-layer, viscoelastic, anisotropic targets, without and with layer-stripping; layer stripping provides faster convergence to better solutions. Finally, an inversion is run with white Gaussian noise (generated using Matlab function wgn) added to the data. Noise is added as a percentage of the largest amplitude in the $\tau$-p seismic data of the model. The maximum number of parameters for the viscoelastic inversions for each layer is seven [P-wave velocity ($V_P$), S-wave velocity ($V_S$), density ($\rho$), layer thickness (h), P-wave quality factor ($Q_P$), S-wave quality factor ($Q_S$) and TI anisotropy factor (PR)]. An option includes application of upper and lower bounds to any or all of these parameters; it works for all combinations of acoustic, elastic, viscoacoustic or viscoelastic, and isotropic or anisotropic data and models.

## RESULTS FOR ELASTIC ANISOTROPIC INVERSIONS

### One elastic target layer

A four layer model (Fig. 2) was created for the elastic inversions, with three fixed shale layers and one target gas sand layer with 90% gas saturation and 10% water saturation. The first example of anisotropic inversion is for data from an anisotropic elastic model with a target gas-sand layer of -10% (HTI) anisotropy (PR = 0.9). The orientation of the symmetry axis for the HTI model is horizontal and within the model plane that also contains the source and the line of receivers; thus the P-S converted waves are quasi-SV waves. The target model is used to generate the test data and contains the parameter values we want to get back from the inversion, beginning with the starting model. Results from this inversion (Fig. 3 and Table 1) show that anisotropic inversion is able to accurately recover the target model values. Synthetic data (Fig. 3) for the target model, the starting model, and the SVD final inverted model, show very small residuals (the difference between the observed and predicted data for the final model), at the final (62nd) iteration. Table 1 contains the differences between the anisotropic and isotropic elastic inversions of the data with [−10%] anisotropy. The numbers on the second line in the solution boxes are the % error in the corresponding estimated parameters, at convergence; the errors are ~0% for the anisotropic inversion and 2% to 15% for the isotropic inversion.

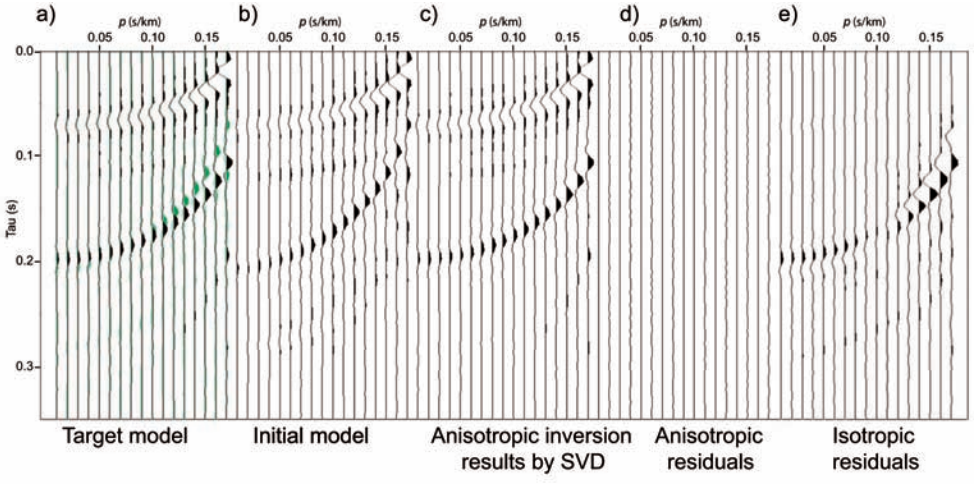


Fig. 3. Seismograms (a, b, c) and residuals (d) of an anisotropic inversion and residuals (e) of an isotropic inversion, of synthetic data from an anisotropic elastic model with a target layer of [−10%] anisotropy. The green traces in (a) are for the initial model, to compare with those of the data for the target model (the black traces). The data being inverted are the same for both inversions. Residuals (d) are after 62 iterations, and (e), after 50 iterations. p is slowness; tau ($\tau$) is intercept time.

Table 1. Summary of final inversion estimations for anisotropic (HTI) and isotropic elastic models with a target layer of [−10%] anisotropy (90% gas sand). The starting model for the isotropic inversion has the same values as the starting model for the anisotropic model except for anisotropic factor, which is fixed at 1.00 (isotropic) for the target layer. The values on the line below the starting and inverted values for the final isotropic and anisotropic models are the (%) errors relative to the known model. The RMS errors are the errors of fitting of the seismogram data.

| Target Layer | Vp (km/s) | Vs (km/s) | $\rho$ (g/cm$^3$) | Thickness (km) | Aniso. Factor | RMS error |
|---|---|---|---|---|---|---|
| Target values (-10%) | 2.543 | 1.597 | 2.090 | 0.160 | 0.900 | |
| Starting model (Aniso.) | 2.653 | 1.897 | 2.150 | 0.180 | 0.950 | |
| | 4.33% | 18.79% | 2.87% | 12.50% | 5.56% | |
| Final Aniso. (-10%) | 2.543 | 1.597 | 2.090 | 0.160 | 0.900 | 0.23242E-06 |
| | 0.00% | 0.00% | 0.00% | 0.00% | 0.00% | |
| Starting model (Iso.) | 2.653 | 1.897 | 2.150 | 0.180 | 1.000 | |
| | 4.33% | 18.79% | 2.87% | 12.50% | 11.11% | |
| Final Iso. (-10%) | 2.676 | 1.825 | 2.133 | 0.184 | 1.000 | 0.15123E-01 |
| | 5.23% | 14.28% | 2.06% | 15.00% | 11.11% | |

The next example is for the same target model and anisotropic data, but assumes and inverts for, an isotropic target layer. This inversion is not convergent (Fig. 3e). The estimated values after 50 iterations are still far from the correct ones; there are large residuals between the target and the final inversion parameters (and between the corresponding wavefields in Fig. 3e). The RMS errors between the observed and predicted seismic traces (Table 1), calculated at the final iteration are five orders of magnitude smaller for the anisotropic inversion (Fig. 3d) than for the isotropic (Fig. 3e).

In the parameter correlation matrix for the anisotropic inversion (Fig. 4a) there are positive correlations between $V_P$, $V_S$, thickness and anisotropy, and inverse correlations between $V_P$ and density, and $V_S$ and density, all as expected. For example, the negative correlation between $V_P$ and density is a consequence of maintaining a constant P-wave impedance ($\rho V_P$). For the isotropic inversion of the anisotropic data (Fig. 4b), the parameters correlate primarily with themselves and $V_P$ correlates with thickness. Parameters are not interacting physically as they should, because of the lack of an anisotropic parameter in the solution forces unreasonable relations between the remaining parameters (Tiwari and McMechan, 2007a).

Using the same procedure, an inversion is performed for a similar model, but with a +10% (VTI) anisotropic target layer; anisotropic inversion is able to recover accurate values of all parameters (Table 2) with small residuals. For the isotropic inversion of the same data from the same starting model, but assuming an isotropic model, the inversion again does not converge to the right values (Table 2) and produces very large residuals, as in the previous isotropic inversion. Table 2 summarizes the corresponding results of anisotropic and isotropic inversions for +10% anisotropy. The results of anisotropic inversion

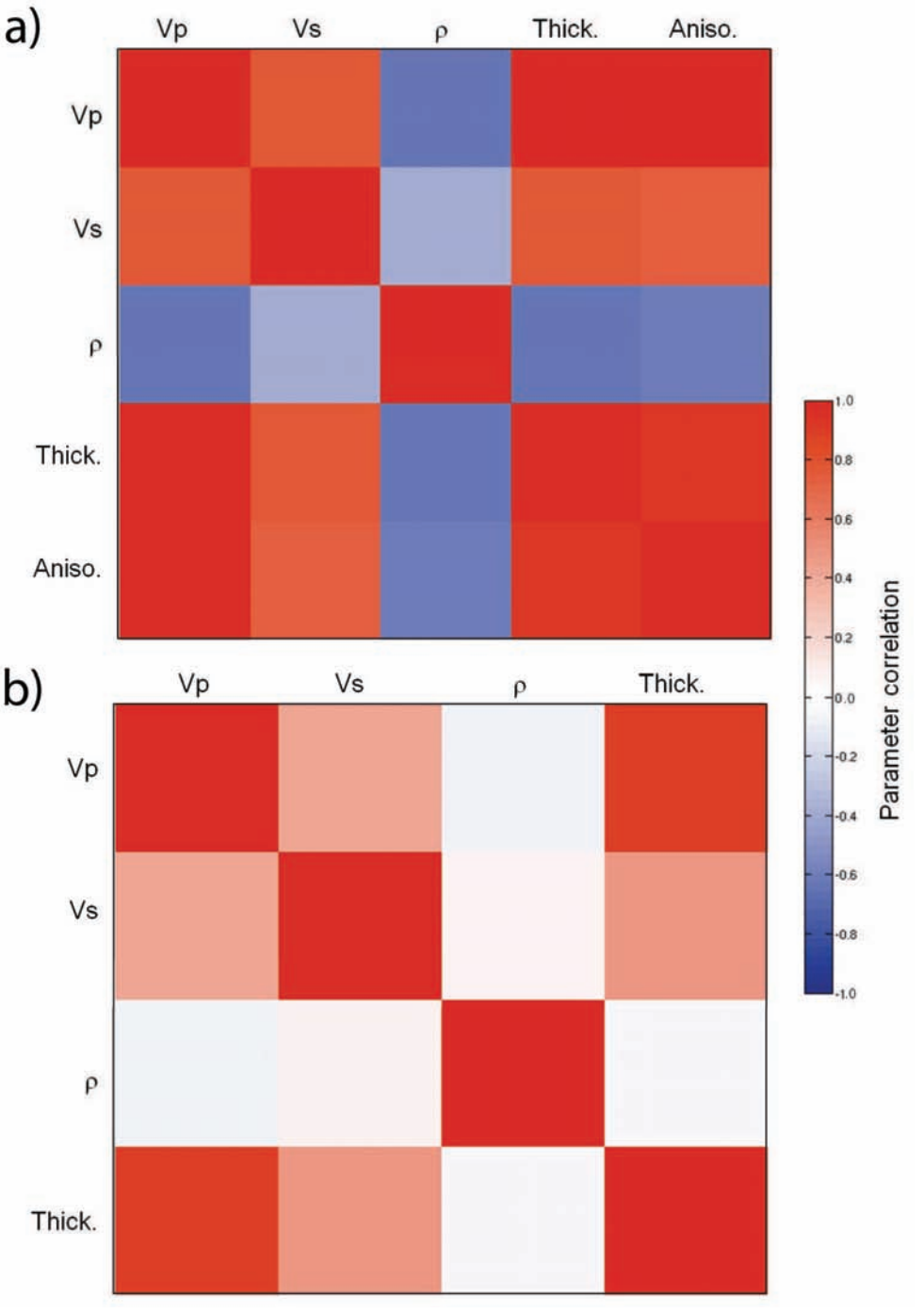


Fig. 4. Parameter correlation matrices for the (a) anisotropic, and (b) isotropic, inversions of synthetic data from an anisotropic elastic model with a target layer of [−10%] anisotropy.

Table 2. Summary of final inverted parameters for anisotropic and isotropic elastic models with a target layer of [+10%] anisotropy. The lithology is 90% gas sand. The starting model for the isotropic inversion has the same values as the starting model for the anisotropic model except for anisotropic factor, which is fixed at 1.00 (isotropic) for the target layer. (See definition of the model and data errors in the caption to Table 1).

| Target Layer | Vp (km/s) | Vs (km/s) | $\rho$ (g/cm$^3$) | Thickness (km) | Aniso. Factor | RMS error |
|---|---|---|---|---|---|---|
| Target values (+10%) | 2.543 | 1.597 | 2.090 | 0.160 | 1.100 | |
| Starting model (Aniso.) | 2.653 | 1.897 | 2.150 | 0.180 | 1.050 | |
| | 4.33% | 18.79% | 2.87% | 12.50% | 4.55% | |
| Final Aniso. (+10%) | 2.543 | 1.597 | 2.090 | 0.160 | 1.100 | 0.19465E-06 |
| | 0.00% | 0.00% | 0.00% | 0.00% | 0.00% | |
| Starting model (Iso.) | 2.653 | 1.897 | 2.150 | 0.180 | 1.000 | |
| | 4.33% | 18.79% | 2.87% | 12.50% | 9.09% | |
| Final Iso. (+10%) | 2.677 | 1.300 | 2.198 | 0.198 | 1.000 | 0.12913E-01 |
| | 5.27% | 18.60% | 5.17% | 23.75% | 9.09% | |

are close to the correct solution with near zero residuals, but isotropic inversion has large (between 5% and 24%) errors. Data for models of more layers and lower (like 5%) anisotropy (not shown here) have slightly smaller errors in the anisotropic inversion than for 10% anisotropy.

## Three elastic target layers

In this section, elastic anisotropic inversions for synthetic elastic anisotropic data for models with three target layers are performed; the sequence to be inverted is sand, shale and sand. For the first example, we use $-10\%$ (HTI) sand anisotropy and $+5\%$ (VTI) shale anisotropy. The resulting parameter errors from the anisotropic inversion (Table 3) increase with each successively deeper layer, but the residual wavefields are still small (Fig. 5d). It also now takes more iterations to converge than for the single layer models. A few of the fitted model parameters have errors larger than those in the starting model, but the largest error is still only 2.76%; this is remedied by using layer stripping, as illustrated in the following section. For isotropic inversion of the same three-layer anisotropic data, the residual errors of the values (Table 3) are larger than for the anisotropic inversion, and the wavefield residuals are much larger (Fig. 5e).

The parameter correlation matrix for the anisotropic solution (Fig. 6a) shows strong correlation within each layer, and much smaller between layers. Also, it shows that parameters within each of the three layers correlate differently and there are more complicated correlations between layers as they get deeper. Additionally, correlations within the first layer are nearly identical to the single layer ones in Fig. 4b. The parameter correlation matrix in Fig. 6b

(for the isotropic solution) shows more correlation between layers than in Fig. 6a. If the model parametrization is correct for the data being inverted, the correlation between parameters within each layer should be substantially larger than those between layers. It also shows very similar correlations between the parameters in the first layer to those for the single isotropic layer model in Fig. 4b. The RMS errors in the isotropic inversion (0.16795E-01) are two orders of magnitude larger than for the anisotropic inversion (0.51391E-03). RMS errors are for the inversion of all three target layers combined. The results for anisotropic inversion are still acceptable ($< 3\%$ error) [Table 3, and in the residual wavefield (Fig. 5d)].

Table 3. Summary of final inverted parameters for anisotropic and isotropic elastic model with three target layers; two 90% gas sands of [-10%] anisotropy (layers 3 and 5) and a shale of [+5%] anisotropy (layer 4). The starting model for the isotropic inversion has the same values as the starting model for the anisotropic model except for anisotropic factor, which is fixed at 1.00 (isotropic) for the target layers. (See definition of the model and data errors in the caption of Table 1).

| Target Layer | Vp (km/s) | Vs (km/s) | $\rho$ (g/cm$^3$) | Thickness (km) | Aniso. Factor |
|---|---|---|---|---|---|
| Target values (-10%) (Layer 3) | 2.543 | 1.597 | 2.090 | 0.160 | 0.900 |
| Target values (+5%) (Layer 4) | 2.825 | 1.202 | 2.275 | 0.100 | 1.050 |
| Target values (-10%) (Layer 5) | 2.543 | 1.597 | 2.090 | 0.160 | 0.900 |
| Starting model (Aniso.) (Layer 3) | 2.653<br>4.33% | 1.897<br>18.79% | 2.150<br>2.87% | 0.170<br>6.25% | 0.950<br>5.56% |
| Starting model (Aniso.) (Layer 4) | 2.850<br>0.88% | 1.150<br>4.33% | 2.250<br>1.10% | 0.110<br>10.00% | 1.070<br>1.90% |
| Starting model (Aniso.) (Layer 5) | 2.553<br>0.39% | 1.697<br>6.26% | 2.150<br>2.87% | 0.150<br>6.25% | 0.920<br>2.22% |
| Final Aniso. (-10%) (Layer 3) | 2.565<br>0.87% | 1.607<br>0.63% | 2.078<br>0.57% | 0.161<br>0.63% | 0.894<br>0.67% |
| Final Aniso. (+5%) (Layer 4) | 2.756<br>2.44% | 1.178<br>2.00% | 2.310<br>1.54% | 0.099<br>1.00% | 1.079<br>2.76% |
| Final Aniso. (-10%) (Layer 5) | 2.473<br>2.75% | 1.555<br>2.63% | 2.129<br>1.87% | 0.156<br>2.50% | 0.916<br>1.78% |
| Final Iso. (-10%) (Layer 3) | 2.769<br>8.89% | 2.163<br>35.44% | 2.015<br>3.59% | 0.181<br>13.13% | 1.000<br>11.11% |
| Final Iso. (+5%) (Layer 4) | 2.734<br>3.22% | 1.700<br>41.43% | 2.460<br>8.13% | 0.093<br>7.00% | 1.000<br>4.76% |
| Final Iso. (-10%) (Layer 5) | 2.610<br>2.63% | 1.235<br>22.67% | 2.080<br>0.48% | 0.170<br>6.25% | 1.000<br>11.11% |

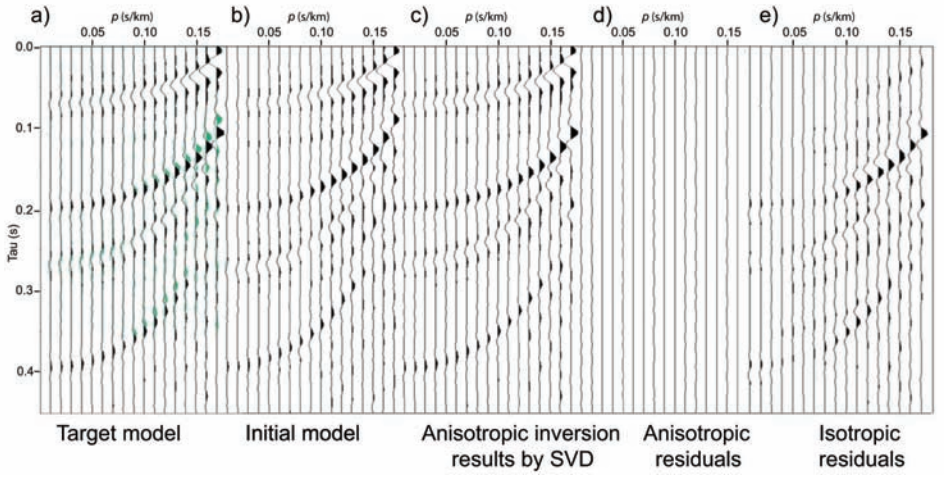


Fig. 5. Seismograms (a, b, c) and residuals (d) of an anisotropic inversion, and residuals (e) of an isotropic inversion, of synthetic data from an anisotropic elastic model with three target layers; two sands of [−10%] anisotropy and a shale of [+5%] anisotropy. The green traces in (a) are for the initial model, to compare with those of the data for the target model (the black traces). The data being inverted are the same for both inversions. Residuals (d) and (e) are both after 80 iterations. p is slowness; tau ($\tau$) is intercept time.

## RESULTS FOR VISCOELASTIC ANISOTROPIC INVERSIONS WITH LAYER STRIPPING

It gets more difficult to simultaneously estimate all parameters as more layers and more parameters are added to a model. Therefore, the inversions in this section are performed with layer stripping [solving for one layer (for noise free data), or for two adjacent layers at a time (for noisy data)]. Stripping proceeds downward from the shallower target layer; the starting model for each layer contains the best-fit solution for the shallower layers. The examples below compare results of viscoelastic anisotropic inversions, with and without layer stripping, for data from viscoelastic, anisotropic models with three target layers (two 90% gas sands and one shale). The target and starting models are similar to the three-layer elastic models in the three target layer section above, but add quality factors $Q_P$ and $Q_S$ to the target layers (Table 4).

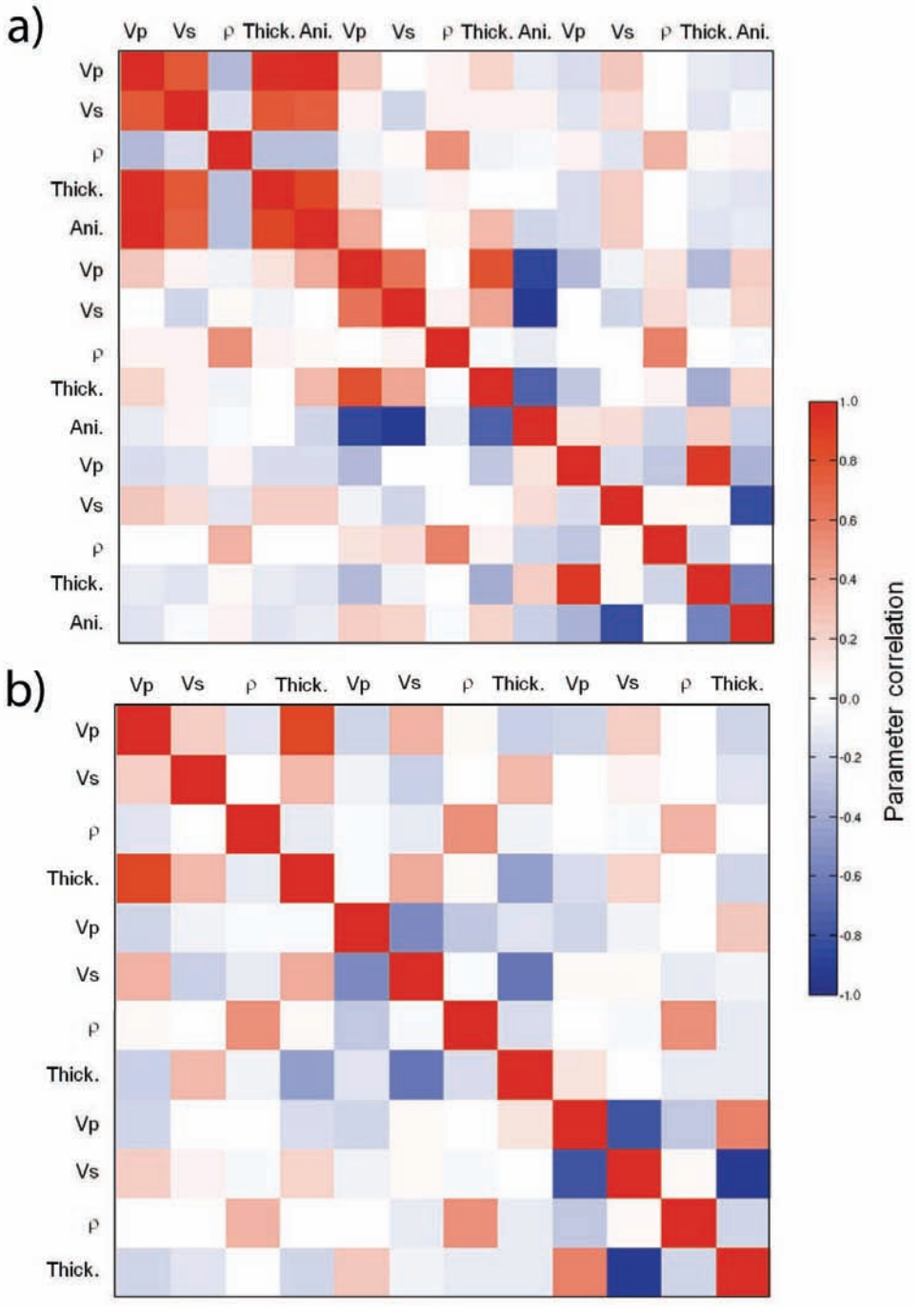


Fig. 6. Parameter correlation matrices for the (a) anisotropic and (b) isotropic inversions, of synthetic data from an anisotropic elastic model with three target layers; two sands of [−10%] anisotropy (the first sand is the first third of the diagonal, the second sand is the last third of the diagonal) and a shale of [+5%] anisotropy is on the middle third of the diagonal.

## Viscoelastic anisotropic inversions with and without layer stripping for HTI sands with 20% noise

The first viscoelastic example has $-10\%$ anisotropy (PR = 0.9) in the sand and $+5\%$ in the shale, and the inversion is anisotropic viscoelastic (Table 4). The final estimations (the best fit from the final SVD iteration, using layer stripping) occur after twelve CG iterations for first target layer, and nine iterations for each of the second and third target layers. The inversion results are close to the target model and they show small residuals (Table 5 and Fig. 7d).

Table 4. Target and starting models for inversion of viscoelastic anisotropic data. The model contains three target layers; two 90% gas sands of [−10%] (HTI) anisotropy (layers 3 and 5) and a shale of [+5%] anisotropy (VTI) (layer 4).

| Target Layer | Vp (km/s) | Vs (km/s) | $\rho$ (g/cm$^3$) | Thickness (km) | $\log_2$Qp | $\log_2$Qs | Aniso. Factor |
|---|---|---|---|---|---|---|---|
| Target values (-10%) (Layer 3) | 2.543 | 1.597 | 2.090 | 0.160 | 5.933 | 4.838 | 0.900 |
| Target values (+5%) (Layer 4) | 2.825 | 1.202 | 2.275 | 0.100 | 6.629 | 4.926 | 1.050 |
| Target values (-10%) (Layer 5) | 2.543 | 1.597 | 2.090 | 0.160 | 5.933 | 4.838 | 0.900 |
| Starting model (Aniso.) (Layer 3) | 2.653<br>4.33% | 1.897<br>18.79% | 2.150<br>2.87% | 0.170<br>6.25% | 6.140<br>3.49% | 4.733<br>2.17% | 0.950<br>5.56% |
| Starting model (Aniso.) (Layer 4) | 2.850<br>0.88% | 1.150<br>4.33% | 2.250<br>1.10% | 0.110<br>10.00% | 6.615<br>0.21% | 5.018<br>1.87% | 1.070<br>1.90% |
| Starting model (Aniso.) (Layer 5) | 2.553<br>0.39% | 1.697<br>6.26% | 2.100<br>0.48% | 0.150<br>6.25% | 5.980<br>0.79% | 4.935<br>2.00% | 0.920<br>2.22% |

The next example uses the same anisotropic target and starting models in Table 4, but are inverted without layer stripping; all parameters for all layers are inverted simultaneously with CG and with a final iteration with SVD. The final residuals are small (Fig. 7e), but they are everywhere larger than those obtained by layer stripping (Table 5). The correlation matrix for the solution without layer stripping (Fig. 8) shows stronger correlation between parameters within each layer, with very little correlation between the layers. Layer four correlates most with the others, because it is in the middle and so interacts with both layers 3 and 5. The layer stripping solution converges in fewer iterations (most of the time) and gives smaller errors for all parameters except $Q_P$ in layer 4, and smaller RMS errors in all three target layers (Table 5). The RMS errors for the layer stripping solution are smaller by about one order of magnitude than those without layer stripping. The viscoelastic anisotropic inversion solution with layer stripping is better than that without layer stripping (Table 5).

| Target Layer | Vp (km/s) | Vs (km/s) | $\rho$ (g/cm$^3$) | Thickness (km) | $\log_2$Qp | $\log_2$Qs | Aniso. Factor | RMS error |
|---|---|---|---|---|---|---|---|---|
| Final Aniso. (-10%) LS | 2.544 | 1.600 | 2.089 | 0.160 | 5.947 | 4.853 | 0.900 | 0.16314E-04 |
| (Layer 3) | 0.04% | 0.19% | 0.05% | 0.00% | 0.24% | 0.31% | 0.00% | |
| Final Aniso. (+5%) LS | 2.817 | 1.203 | 2.275 | 0.100 | 6.547 | 4.921 | 1.051 | 0.57709E-04 |
| (Layer 4) | 0.28% | 0.08% | 0.00% | 0.00% | 1.24% | 0.10% | 0.10% | |
| Final Aniso. (-10%) LS | 2.527 | 1.570 | 2.098 | 0.159 | 5.924 | 4.689 | 0.904 | 0.12266E-03 |
| (Layer 5) | 0.63% | 1.69% | 0.38% | 0.63% | 0.16% | 3.07% | 0.44% | |
| Final Aniso. (-10%) w/o LS | 2.555 | 1.594 | 2.085 | 0.160 | 5.966 | 4.787 | 0.898 | 0.22429E-03 |
| (Layer 3) | 0.47% | 0.19% | 0.24% | 0.00 % | 0.55% | 1.06% | 0.22% | |
| Final Aniso. (+5%) w/o LS | 2.769 | 1.192 | 2.308 | 0.098 | 6.647 | 5.005 | 1.075 | 0.22429E-03 |
| (Layer 4) | 1.98% | 0.83% | 1.45% | 2.00% | 0.26% | 1.59% | 2.38% | |
| Final Aniso. (-10%) w/o LS | 2.515 | 1.737 | 2.109 | 0.158 | 5.952 | 7.229 | 0.906 | 0.22429E-03 |
| (Layer 5) | 1.10% | 8.77% | 0.91% | 1.25% | 0.32% | 49.42% | 0.67% | |
| Final Aniso. (-10%) LS | 2.543 | 1.597 | 2.090 | 0.160 | 5.933 | 4.838 | 0.900 | 0.10798E-05 |
| $2^{nd}$ run (Layer 3) | 0.00% | 0.00% | 0.00% | 0.00% | 0.00% | 0.00% | 0.00% | |
| Final Aniso. (+5%) LS | 2.823 | 1.202 | 2.275 | 0.100 | 6.624 | 4.921 | 1.051 | 0.13165E-04 |
| $2^{nd}$ run (Layer 4) | 0.07% | 0.00% | 0.00% | 0.00% | 0.09% | 0.10% | 0.10% | |
| Final Aniso. (-10%) LS | 2.542 | 1.602 | 2.091 | 0.160 | 5.933 | 4.883 | 0.900 | 0.37096E-04 |
| $2^{nd}$ run (Layer 5) | 0.04% | 0.31% | 0.05% | 0.00% | 0.00% | 0.92% | 0.00% | |
| Final Aniso. (-10%) w/o LS | 2.553 | 1.595 | 2.086 | 0.160 | 5.959 | 4.797 | 0.898 | 0.22718E-03 |
| $2^{nd}$ run (Layer 3) | 0.39% | 0.13% | 0.19% | 0.00% | 0.43% | 0.85% | 0.22% | |
| Final Aniso. (+5%) w/o LS | 2.769 | 1.193 | 2.308 | 0.098 | 6.660 | 5.009 | 1.075 | 0.22718E-03 |
| $2^{nd}$ run (Layer 4) | 1.98% | 0.75% | 1.45% | 2.00% | 0.46% | 1.68% | 2.38% | |
| Final Aniso. (-10%) w/o LS | 2.513 | 1.735 | 2.110 | 0.158 | 5.938 | 7.219 | 0.906 | 0.22718E-03 |
| $2^{nd}$ run (Layer 5) | 1.18% | 8.64% | 0.96% | 1.25% | 0.08% | 49.22% | 0.67% | |

Table 5. Summary of final anisotropic viscoelastic inversions with and without layer stripping (LS) and with first and second run results for the viscoelastic anisotropic target model in Table 4. The RMS errors for the non-stripping solution are the same for all three layers as separate values for each layer are not obtainable when they are estimated as a single composite model. (See definition of the model and data errors in the caption to Table 1).

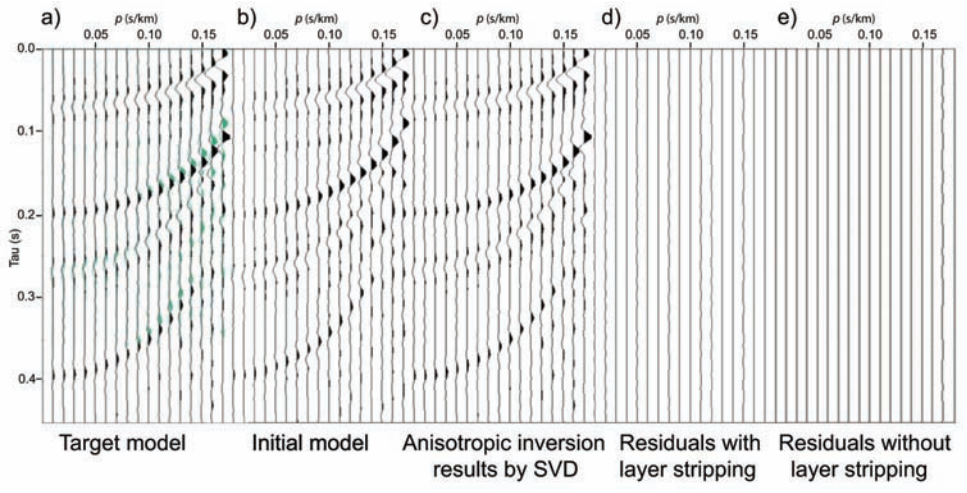


Fig. 7. Seismograms (a, b, c) and residuals of an anisotropic viscoelastic inversion (d) with layer stripping, and (e) without layer stripping, using synthetic data from an anisotropic viscoelastic model with three target layers; two sands of [−10%] anisotropy and a shale of [+5%] anisotropy. The green traces in (a) are for the initial model, to compare with those of the data for the target model (the black traces). The data being inverted are the same for both inversions. Residuals (d) are after 12, 9, and 9 iterations for target layers 3, 4 and 5, respectively, for inversions with layer stripping; (e) is after 50 iterations without layer stripping. p is slowness; tau ($\tau$) is intercept time.

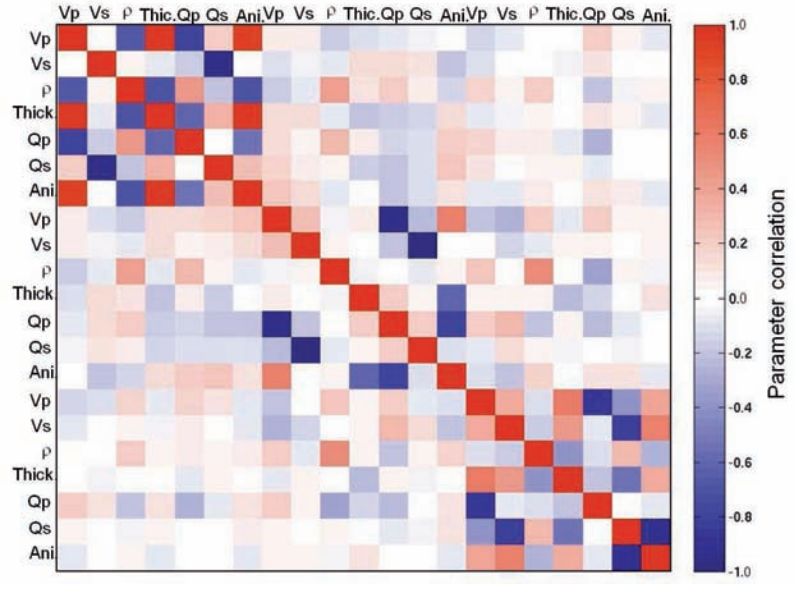


Fig. 8. Parameter correlation matrix for the anisotropic viscoelastic inversion without layer stripping of synthetic data from an anisotropic viscoelastic model with three target layers; two sands of [−10%] anisotropy [the first sand (layer 3) is the first third of the diagonal, the second sand (layer 5) is the last third of the diagonal, and a shale of [+5%] anisotropy (layer 4) is on the middle third of the diagonal].

A second run of layer stripping inversion was performed for the model of −10% anisotropic sands and +5% anisotropic shale, taking the final result from the first layer stripping inversion as the starting model, and layer stripping again from the top down. Residuals for the second run with layer stripping (Fig. 9d and Table 5), are significantly better than after the first run. The RMS errors are one order of magnitude less for the second run than for the first; most of the parameter errors are almost zero and all of them are less than 1%. A second inversion run without layer stripping was also performed (Fig. 9e); this does not show as much improvement as with layer stripping (Table 5). Without layer stripping, the number of iterations required to converge in the second pass are a lot less than those in the first pass. The RMS errors are 1 to 2 orders of magnitude less with layer stripping, in both the first and second passes, than without layer stripping.

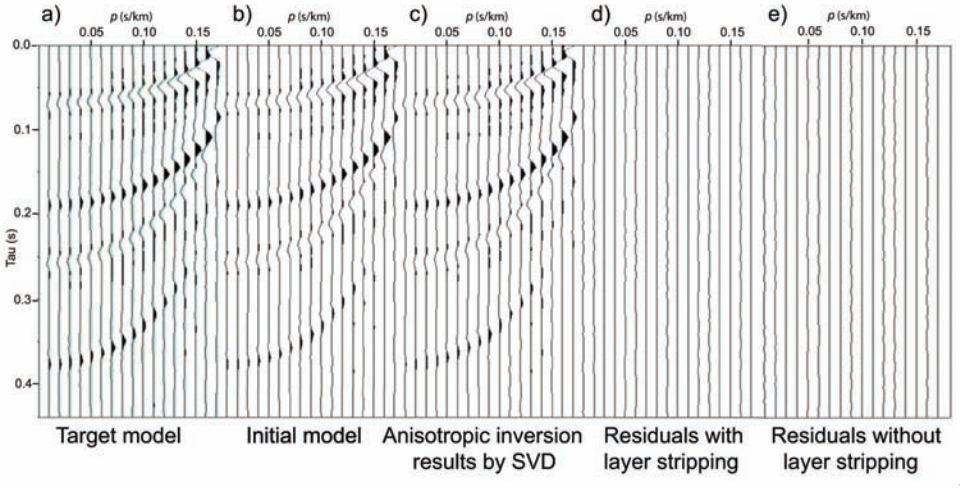


Fig. 9. Seismograms (a, b, c) and residuals of a second run of anisotropic viscoelastic inversion with layer stripping of the final result from the first inversion as the starting model. The data are from an anisotropic viscoelastic model with three target layers; two sands of [−10%] anisotropy and a shale of [+5%] anisotropy. The green traces in (a) are for the initial model, to compare with those of the data for the target model (the black traces). Residuals (d) are after 7, 27, and 16 iterations for target layers 3, 4 and 5 respectively, with layer stripping, and residuals (e) are after 13 iterations without layer stripping. p is slowness; tau ($\tau$) is intercept time.

## Viscoelastic anisotropic inversions with and without layer stripping for VTI sands

In this next example, the three layer target model has +10% anisotropy in the sands and +5% anisotropy in the shale. All the other parameters are the same as those in Table 4, except the starting estimates of PR in layers 3, 4 and

5 are 1.050, 1.030 and 1.080 respectively (Table 6). This model was inverted with and without layer stripping; the result from the layer stripping inversion for this model shows smaller residuals (Fig. 10d and Table 7) than the solution without layer stripping (Fig. 10e and Table 7).

Table 6. Target and starting models for inversion of viscoelastic anisotropic data. The model contains three VTI target layers; two 90% gas sands of [+10%] anisotropy (layers 3 and 5) and a shale of [+5%] anisotropy (layer 4).

| Target Layer | Vp (km/s) | Vs (km/s) | $\rho$ (g/cm$^3$) | Thickness (km) | $\log_2$Qp | $\log_2$Qs | Aniso. Factor |
|---|---|---|---|---|---|---|---|
| Target values (+10%) (Layer 3) | 2.543 | 1.597 | 2.090 | 0.160 | 5.933 | 4.838 | 1.100 |
| Target values (+5%) (Layer 4) | 2.825 | 1.202 | 2.275 | 0.100 | 6.629 | 4.926 | 1.050 |
| Target values (+10%) (Layer 5) | 2.543 | 1.597 | 2.090 | 0.160 | 5.933 | 4.838 | 1.100 |
| Starting model (Aniso.) (Layer 3) | 2.653<br>4.33% | 1.897<br>18.79% | 2.150<br>2.87% | 0.170<br>6.25% | 6.140<br>3.49% | 4.733<br>2.17% | 1.050<br>5.00% |
| Starting model (Aniso.) (Layer 4) | 2.850<br>0.88% | 1.150<br>4.33% | 2.250<br>1.10% | 0.110<br>10.00% | 6.615<br>0.21% | 5.018<br>1.87% | 1.030<br>1.90% |
| Starting model (Aniso.) (Layer 5) | 2.553<br>0.39% | 1.697<br>6.26% | 2.100<br>0.48% | 0.150<br>6.25% | 5.980<br>0.79% | 4.935<br>2.00% | 1.080<br>1.80% |

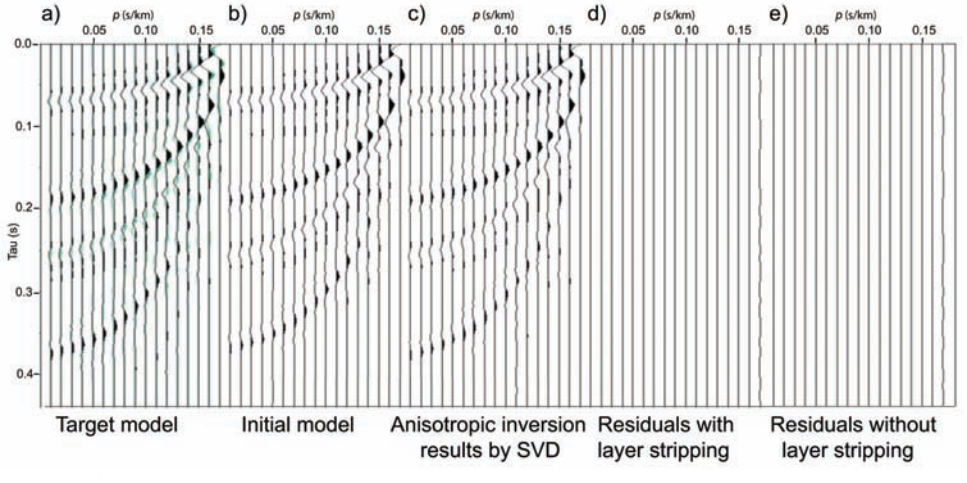


Fig. 10. Seismograms (a, b, c) and residuals of an anisotropic viscoelastic inversion (d) with and (e) without layer stripping, using synthetic data from an anisotropic viscoelastic model with three target layers; two sands of [+10%] anisotropy and a shale of [+5%] anisotropy. The green traces in (a) are for the initial model, to compare with those of the data for the target model (the black traces). Residuals (d) are after 12, 29, and 7 iterations for target layers 3, 4 and 5 respectively, and residuals (e) are after 41 iterations without layer stripping. p is slowness; tau ($\tau$) is intercept time.

| Target Layer | Vp (km/s) | Vs (km/s) | $\rho$ (g/cm$^3$) | Thickness (km) | $\log_2$Qp | $\log_2$Qs | Aniso. Factor | RMS error |
|---|---|---|---|---|---|---|---|---|
| Final Aniso. (+10%) LS | 2.544 | 1.599 | 2.089 | 0.160 | 5.943 | 4.848 | 1.100 | 0.14694E-04 |
| (Layer 3) | 0.04% | 0.13% | 0.05% | 0.00% | 0.16% | 0.21% | 0.00% | |
| Final Aniso. (+5%) LS | 2.829 | 1.199 | 2.275 | 0.100 | 6.698 | 4.883 | 1.050 | 0.26088E-04 |
| (Layer 4) | 0.14% | 0.25% | 0.00% | 1.00% | 1.03% | 0.88% | 0.00% | |
| Final Aniso. (+10%) LS | 2.491 | 1.681 | 2.109 | 0.159 | 5.797 | 4.921 | 1.105 | 0.58823E-03 |
| (Layer 5) | 2.04% | 5.26% | 0.91% | 0.63% | 2.29% | 1.72% | 0.45% | |
| Final Aniso. (+10%) w/o LS | 2.559 | 1.603 | 2.097 | 0.159 | 5.928 | 4.935 | 1.107 | 0.27525E-03 |
| (Layer 3) | 0.63% | 0.38% | 0.33% | 0.63% | 0.08% | 2.02% | 0.64% | |
| Final Aniso. (+5%) w/o LS | 2.869 | 1.212 | 2.250 | 0.101 | 6.541 | 4.858 | 1.030 | 0.27525E-03 |
| (Layer 4) | 1.56% | 0.83% | 1.10% | 1.00% | 1.34% | 1.38% | 1.90% | |
| Final Aniso. (+10%) w/o LS | 2.608 | 1.556 | 2.058 | 0.163 | 6.002 | 4.372 | 1.074 | 0.27525E-03 |
| (Layer 5) | 2.56% | 2.57% | 1.53% | 1.88% | 1.17% | 9.64% | 2.36% | |
| Final Aniso. (+10%) LS | 2.543 | 1.597 | 2.090 | 0.160 | 5.933 | 4.838 | 1.100 | 0.67184E-06 |
| $2^{nd}$ run (Layer 3) | 0.00% | 0.00% | 0.00% | 0.00% | 0.00% | 0.00% | 0.00% | |
| Final Aniso. (+5%) LS | 2.825 | 1.202 | 2.275 | 0.100 | 6.626 | 4.926 | 1.050 | 0.85506E-05 |
| $2^{nd}$ run (Layer 4) | 0.00% | 0.00% | 0.00% | 0.00% | 0.04% | 0.00% | 0.00% | |
| Final Aniso. (+10%) LS | 2.542 | 1.597 | 2.091 | 0.160 | 5.926 | 4.843 | 1.100 | 0.21195E-04 |
| $2^{nd}$ run (Layer 5) | 0.04% | 0.00% | 0.05% | 0.00% | 0.12% | 0.10% | 0.00% | |
| Final Aniso. (+10%) w/o LS | 2.528 | 1.602 | 2.098 | 0.159 | 5.919 | 4.931 | 1.107 | 0.27336E-03 |
| $2^{nd}$ run (Layer 3) | 0.59% | 0.31% | 0.38% | 0.63% | 0.24% | 1.92% | 0.64% | |
| Final Aniso. (+5%) w/o LS | 2.873 | 1.212 | 2.250 | 0.101 | 6.542 | 4.848 | 1.030 | 0.27336E-03 |
| $2^{nd}$ run (Layer 4) | 1.70% | 0.83% | 1.10% | 1.00% | 1.31% | 1.58% | 1.90% | |
| Final Aniso. (+10%) w/o LS | 2.606 | 1.552 | 2.060 | 0.163 | 5.970 | 4.350 | 1.074 | 0.27336E-03 |
| $2^{nd}$ run (Layer 5) | 2.48% | 2.82% | 1.44% | 1.88% | 0.63% | 10.08% | 2.36% | |

Table 7. Summary of final anisotropic viscoelastic inversions with and without layer stripping (LS) and with first and second runs results for the viscoelastic anisotropic target model in Table 6. The RMS errors for the non-stripping solution are the same for all three layers as separate values for each layer are not obtainable when they are estimated as a single composite model. (See definition of the model and data errors in the caption to Table 1).

Second runs of the inversions with and without layer stripping were made for the model of +10% anisotropic sands and +5% anisotropic shale, taking the final result from the first layer stripping inversion as the starting model for the second. The inversions show similar results as in the previous HTI example. Residuals for the second run with layer stripping (Fig. 11d and Table 7), are significantly better than after the first run; the highest parameter error after the second run is only 0.12%. The second inversion run without layer stripping shows almost no improvement (Fig. 11e and Table 7). The RMS errors are two to three orders of magnitude less with layer stripping than without, in both the first and second passes. The number of iterations required to converge in the second pass are generally only ~ half those in the first pass for both inversions (with and without layer stripping).

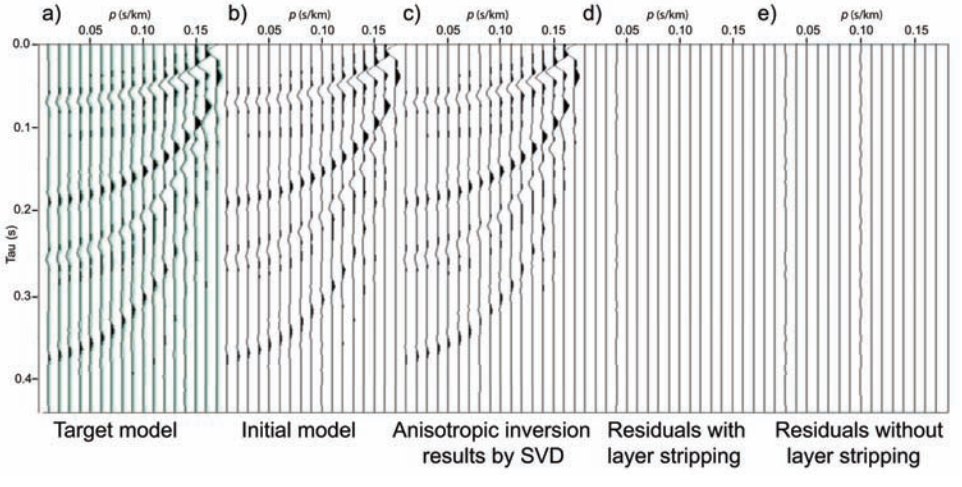


Fig. 11. Seismograms (a, b, c) and residuals of a second run of anisotropic viscoelastic inversion (d) with, and (e) without layer stripping, using the final result from the corresponding first inversion as the starting model. The data are from an anisotropic viscoelastic model with three target layers; two sands of [+10%] anisotropy and a shale of [+5%] anisotropy. The green traces in (a) are for the initial model, to compare with those of the data for the target model (the black traces). Residuals (d) are after 7, 9, and 10 iterations for target layers 3, 4 and 5 respectively, with layer stripping, and residuals (e) are after 20 iterations, without layer stripping. p is slowness; tau ($\tau$) is intercept time.

**Viscoelastic anisotropic inversions with and without layer stripping for HTI sands with 20% noise**

Noise was added to the data for the three-layer HTI sand target model (Table 4). The noise was generated using the white Gaussian noise (wgn) function in Matlab (Fig. 12) and has 20% of the largest amplitude in the $\tau$-p seismic data. The starting model is the same as that in Table 4. The inversion was done with and without layer stripping, as in the previous examples; in both, the layer stripping solves for parameters of each pair of two adjacent layers together, to allow explicit inclusion of the inter-layer interactions across the interface between them. Layer stripping using CG produces slightly improved results compared to using SVD because of the different interaction of the two algorithms with the noise. A second run of this inversion was performed with CG and shows some additional improvement (Table 8); the residual wavefield (Fig. 13) contains the unfitted random noise. While it is more difficult to converge to the correct solution with 20% noise, a maximum parameter error of only 3.30% is obtained for Qs in layer 3 (Table 8). Qs is usually the most difficult parameter to solve for.

## DISCUSSION

As the number of layers is increased in anisotropic viscoelastic model inversions, the inversion errors increase progressively with depth; they accumulate from layer to layer. The parameter correlations confirm this observation, showing increased correlations between layers when there are more layers.

Although only a few shallow target layers are in the models used above, this does not limit the number of layers that can be potentially inverted. The present data configuration can be seen as equivalent to the result of downward continuation of the data through an arbitrarily thick overburden, to a position slightly above the target of interest. The layer stripping illustrated above can also be continued through any desired number of target layers.

As the number of parameters (anisotropic, viscoelastic) being solved for increases, it is more difficult to get unique solutions and stable convergence because the solution space has more local minima. Thus, layer stripping provides better solutions, and convergence behaviour, than without it. Running iterative layer stripping more than once further reduces the residual errors, converges in fewer iterations, and to slightly better solutions with CG than with SVD. This is a consequence of the different behaviours of CG and SVD in the presence of noise.

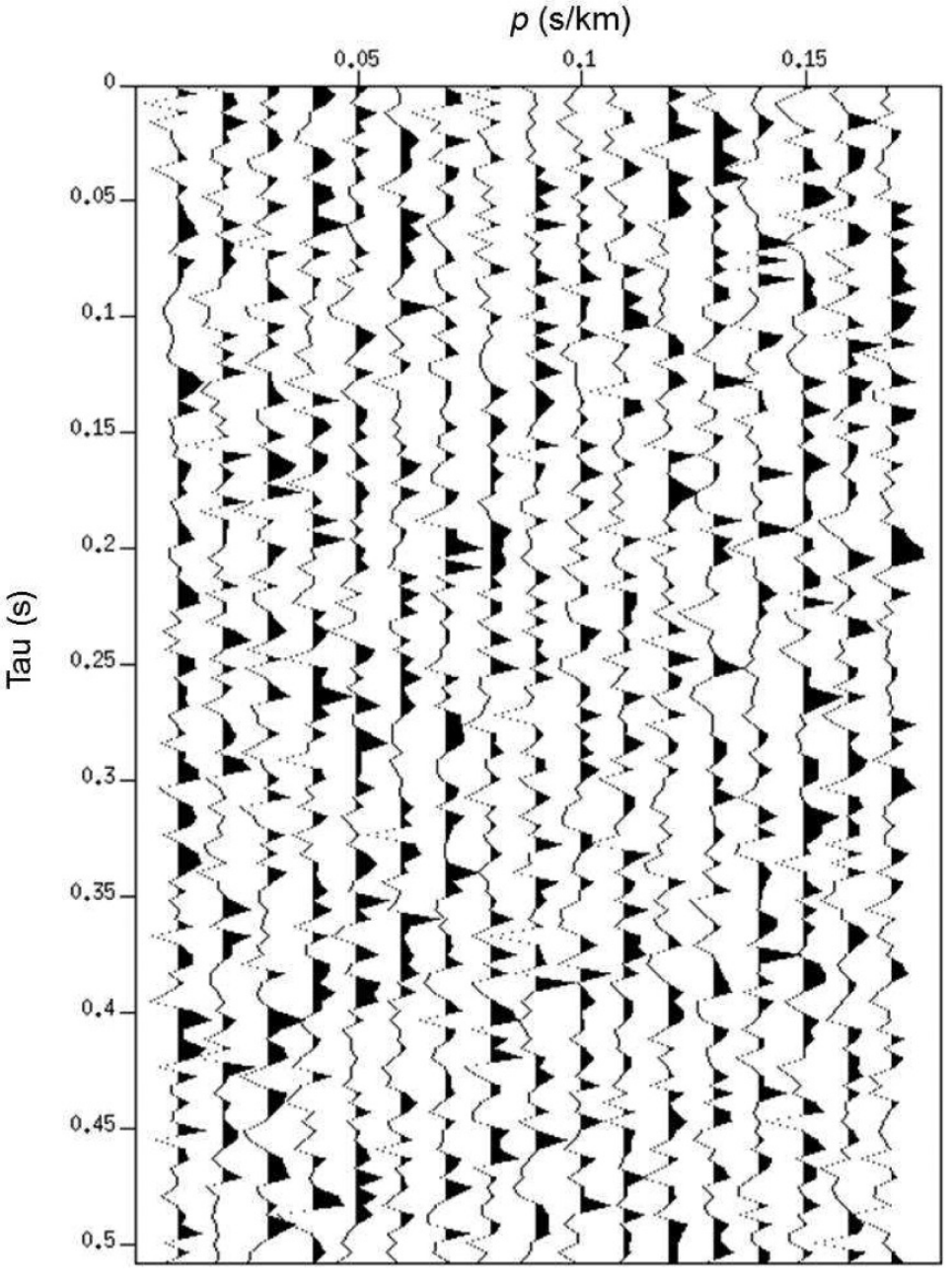


Fig. 12. White Gaussian noise from Matlab scaled and added to the data. p is slowness; tau ($\tau$) is intercept time.

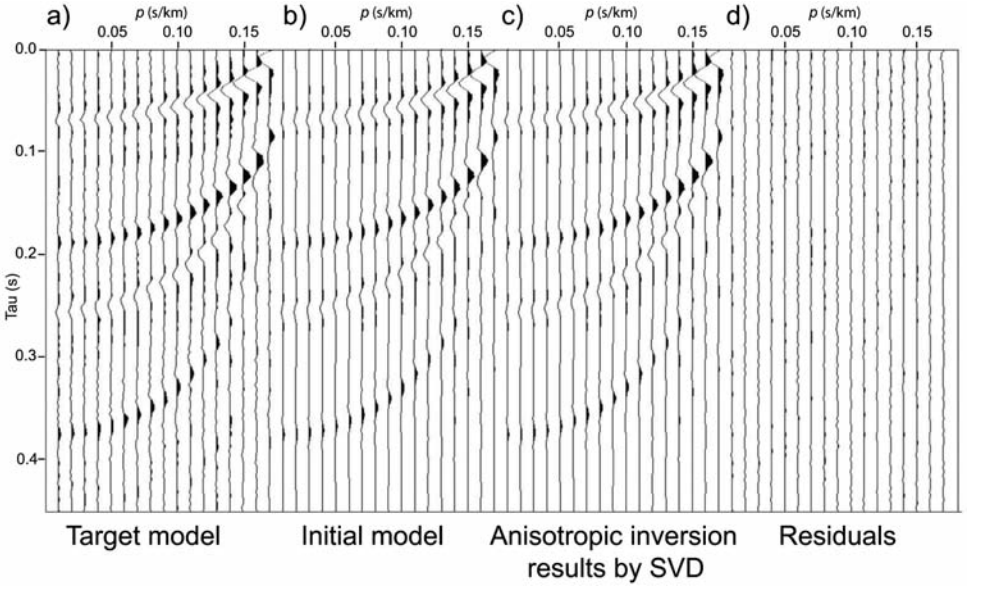


Fig. 13. Seismograms (a, b, c) and residuals (d) of an anisotropic viscoelastic inversion with layer stripping, using synthetic data from an anisotropic viscoelastic model with three target layers; two sands of [−10%] anisotropy and a shale of [+5%] anisotropy with 20% noise. p is slowness; tau ($\tau$) is intercept time.

Isotropic inversion applied to anisotropic data gives slow convergence to wrong model parameters; the anisotropic information in the data gets incorrectly attributed to the isotropic parameters that are solved for, so while convergence may be achieved, it is not possible to get a correct solution for any of the parameters with an incorrect model parametrization.

The parameter correlation matrix in Fig. 8 reveals some interesting relations. The most consistent are the strong negative correlations between $Q_P$ and $V_P$ and between $Q_S$ and $V_S$; these are expected, as Q is parameterized in the reflectivity algorithm as a complex velocity (Schwab and Knopoff, 1972). Other correlations vary from model to model. The residual errors are consistently less than 1% for all parameters, except where inappropriate parameterizations (e.g., isotropic rather than anisotropic) are used, or when layer stripping is not used (and thus the solution is more susceptible to falling into a local minimum), or when noise is added to the data. Even for noisy data (Table 8), after two cycles of layer stripping, only $Q_P$ and $Q_S$ have errors up to 3.3%, which is still acceptable.

| Target Layer | Vp (km/s) | Vs (km/s) | $\rho$ (g/cm$^3$) | Thickness (km) | $\log_2$Qp | $\log_2$Qs | Aniso. Factor | RMS error |
|---|---|---|---|---|---|---|---|---|
| Final Aniso. (-10%) LS | 2.588 | 1.593 | 2.096 | 0.161 | 6.115 | 4.672 | 0.891 | 0.10463E-01 |
| $1^{st}$ run (Layer 3) | 1.77% | 0.25% | 0.29% | 0.63% | 3.06% | 3.42% | 1.00% | |
| Final Aniso. (+5%) LS | 2.798 | 1.204 | 2.287 | 0.100 | 6.594 | 4.950 | 1.063 | 0.10463E-01 |
| $1^{st}$ run (Layer 4) | 0.96% | 0.17% | 0.53% | 0.00% | 0.53% | 0.48% | 1.24% | |
| Final Aniso. (-10%) LS | 2.500 | 1.585 | 2.135 | 0.158 | 5.973 | 4.986 | 0.916 | 0.63511E-02 |
| $1^{st}$ run (Layer 5) | 1.69% | 0.75% | 2.15% | 1.25% | 0.67% | 3.07% | 1.78% | |
| Final Aniso. (-10%) LS | 2.587 | 1.593 | 2.091 | 0.161 | 6.111 | 4.678 | 0.891 | 0.10459E-01 |
| $2^{nd}$ run (Layer 3) | 1.73% | 0.25% | 0.05% | 0.63% | 2.99% | 3.30% | 1.00% | |
| Final Aniso. (+5%) LS | 2.798 | 1.205 | 2.291 | 0.100 | 6.591 | 4.935 | 1.063 | 0.10459E-01 |
| $2^{nd}$ run (Layer 4) | 0.96% | 0.25% | 0.70% | 0.00% | 0.58% | 0.19% | 1.24% | |
| Final Aniso. (-10%) LS | 2.504 | 1.587 | 2.135 | 0.158 | 5.977 | 4.968 | 0.916 | 0.63437E-02 |
| $2^{nd}$ run (Layer 5) | 1.53% | 0.63% | 2.15% | 1.25% | 0.74% | 2.69% | 1.78% | |

Table 8. Summary of final anisotropic viscoelastic inversions with layer stripping (LS) by pairs of adjacent layers, and with first and second run results for the viscoelastic anisotropic target model in Table 4 and with 20% noise added. (See definition of the model and data errors in the caption to Table 1).

The present implementation automatically includes converted waves and internal multiples, but the symmetry axes are confined to the plane of the model, as are the wave polarizations. Thus, the inversion cannot be directly expanded to symmetries with azimuthal effects; a reformulation is necessary. Extension to non-flat (2D or 3D) layer geometries would involve addition of more parameters, as the layer geometry would have to be solved for concurrently, and this would require data from more sources to ensure adequate illumination. For extension to field data, source wavelets would have to be inverted for as well. 3D full-wave inversion also requires a full 3D extrapolation (e.g., Chang and McMechan, 2009a,b) and multicomponent recording. However, it is possible still to use the present form for simulation and inversion of synthetic marine data, as conversions at the water bottom are implicitly included, as the water-to-solid (acoustic-to-elastic) boundary conditions are automatically satisfied. Similarly, air waves can be included by making the upper halfspace air. As the solution is analytical, there are no stability or grid dispersion issues.

The analytic reflectivity integral solution is very efficient. The computations in the examples above took an average of 0.45 s, 0.65 s, and 0.89 s per conjugate gradient iteration for the one, two and three layer inversions, respectively, in one 3.2 GHz Pentium 4 processor. While it is not appropriate in the present form for laterally varying or 3D models, it does, nevertheless, demonstrate that it is possible to overcome the limitations in extracting anisotropy information from traveltimes alone by including amplitudes, it lays the foundation for fitting of models with variable layer shape, and for subsequent inversion (interpretation) of viscoelastic, anisotropic models in terms of sand reservoir properties (e.g., Koesoemadinata and McMechan, 2003; Khazanehdari and McCann, 2005). Substantial future research and development is needed to address these issues.

Although all the models considered here are for shale-bounded, fractured sands, the methodology is general and can be applied to other lithologies. It is anticipated that anisotropy estimation will facilitate characterization of lithology (e.g. shales) and fractures, and that viscoelastic property estimation will facilitates characterization of fluid types and saturations for both exploration and production applications.

## CONCLUSIONS

Combined, simultaneous full wavefield inversion for anisotropic, viscoelastic model parameters is developed and illustrated in the context of synthetic data produced by analytic, frequency-domain, reflectivity solutions for flat-layered models. Provided that the starting models for the inversions satisfy the half-period criterion and the parameterization of the model being solved for

matches that of the input data, the models converge to the correct solution, and all the primary P-P and P-S converted and internal multiple reflections are simultaneously fitted. Layer stripping reduces the number of parameters to be solved for in each sub-inversion, thereby improving computational efficiency; a second pass of layer stripping through the model improves the accuracy of the solution by an order of magnitude, especially for the deeper layers. Including amplitudes in full wave inversion overcomes the nonuniqueness that is inherent in solving for anisotropy parameters using traveltimes alone. Adding noise to the data increases the net wavefield residual at convergence, but does not significantly change the model solution. The results lay the foundation for future viscoelastic anisotropic inversion that also includes lateral structure variations, and for a second inversion to estimate the reservoir properties from the viscoelastic, anisotropic seismic parameters.

## ACKNOWLEDGMENTS

The research leading to this paper was supported by the Sponsors of the UT-Dallas Geophysical Consortium. This paper is Contribution No. 1249 from the Department of Geosciences at The University of Texas at Dallas.

## REFERENCES

Bakker, P.M., 1995. About the completeness of the classification of cases of elliptic anisotropy. Proc. Roy. Soc. London A, 451: 367-373.

Bakulin, A., Woodward, M., Nichols, D., Osypov, K. and Zdraveva, O., 2010. Building tilted transversely isotropic depth models using localized anisotropic tomography with well information. Geophysics, 75(4): D27-D36.

Baraka-Lokmane, S., 2002. Hydraulic versus pneumatic measurements of fractured sandstone permeability. J. Petrol. Sci. Eng., 36: 183-192.

Barbosa, B., Costa, J., Gomes, E. and Schleicher, J., 2008. Resolution analysis for stereotomography in media with elliptic and analeptic anisotropy. Geophysics, 73(4): R49-R58.

Chang, H. and McMechan, G.A., 2009a. 3D, 3-C full wavefield elastic inversion for anisotropic parameters: A feasibility study with synthetic data. Geophysics, 74(6): WCC159-WCC175.

Chang, H. and McMechan, G.A., 2009b. Synthetic data tests of 3D full-wavefield inversion for P-wave anisotropic parameter estimation in flat layered VTI, HTI and orthorhombic media. J. Seismic Explor., 18: 249-270.

Golikov, P. and Stovas, A., 2012. Traveltime parameters in a tilted elliptical anisotropic medium. Geophys. Prosp., 60: 433-443.

Grechka, V., 2009. Nonuniqueness of traveltime inversion in elliptically anisotropic media. Expanded Abstr., 79th Ann. Internat. SEG Mtg., Houston, 28: 196-200.

Guiton, M., Sassi, W., Leroy, Y. and Gauthier, B., 2003. Mechanical constraints on the chronology of fracture activation in folded Devonian sandstone of the western Moroccan Anti-Atlas. J. Struct. Geol., 25: 1317-1330.

Hennings, P., Olson, J. and Thompson, L., 2000. Combining outcrop data and threedimensional structural models to characterize fractured reservoirs: an example from Wyoming. AAPG Bull., 84: 830-849.

Hu, Y. and McMechan, G.A., 2010. Sensitivity of 3-D, 3-C finite-difference elastic seismic data to inclusion parameters in HTI and TTI media with high inclusion density. Geophysics, 75(2): T49-T61.

Kelly, J., Parnell, J. and Chen, H.H., 2000. Application of fluid inclusions to studies of fractured sandstone reservoirs. J. Geochem. Explor., 69-70: 705-709.

Khazanehdari, J. and McCann, C., 2005. Acoustic and petrophysical relationships in low-shale sandstone reservoir rocks. Geophys. Prosp., 53: 447-461.

Kleyn, A.H., 1956. On seismic wave propagation in anisotropic media with applications in the Betun area, south Sumatra. Geophys. Prosp., 4: 56-69.

Koesoemadinata, A.P. and McMechan, G.A., 2001. Empirical estimation of viscoelastic seismic parameters from petrophysical properties of sandstone. Geophysics, 66: 1457-1470.

Koesoemadinata, A.P. and McMechan, G.A., 2003. Petro-seismic inversion for sandstone properties. Geophysics, 68: 1611-1625.

Maultzsch, S., Chapman, M., Liu, E. and Li, X.Y., 2003. Modelling frequency-dependent seismic anisotropy in fluid-saturated rock with aligned fractures: implication of fracture size estimation from anisotropic measurements. Geophys. Prosp., 51: 381-392.

Martínez, R.D. and McMechan, G.A., 1991a. $\tau$-p seismic data for viscoelastic media. Part 1: Modelling. Geophys. Prosp., 39: 141-156.

Martínez, R.D. and McMechan, G.A., 1991b. $\tau$-p seismic data for viscoelastic media. Part 2: Linearized inversion. Geophys. Prosp., 39: 157-182.

Martínez, R.D., 1993. Wave propagation effects on amplitude variation with offset measurements: A study. Geophysics, 58: 534-543.

McCaulay, A.D., 1986. Plane-layer prestack inversion in the presence of surface reverberation. Geophysics, 51: 1789-1800.

Mora, P., 1989. Inversion = migration + tomography. Geophysics, 54: 1575-1586.

Odling, N., Gillespie, P., Bourgine, B., Castaing, C., Chils, J., Christensen, N., Fillion, E., Genter, A., Olsen, C. Thrane, L., Trice, R., Aarseth, E., Walsh, J. and Watterson, J., 1999. Variations in fracture system geometry and their implications for fluid flow in fractured hydrocarbon reservoirs. Petrol. Geosc., 5: 373-384.

Ohlsen, F. and Macbeth, C., 1999. Elliptical anisotropy - regression or advance? Expanded Abstr., 69th Ann. Internat. SEG Mtg., Houston: 1600-1603.

Ortega, O. and Marrett, R., 2000. Prediction of macrofracture properties using microfracture information, Mesaverde Group sandstones, San Juan basin, New Mexico. J. Struct. Geology, 22: 571-588.

Ozdenvar, T. and McMechan, G.A., 1997. Algorithm for staggered grid computations for poroelastic, elastic, acoustic, and scalar wave equations. Geophys. Prosp., 45: 403-420.

Pan, G.S., Phinney, R.A. and Odom, R.I., 1988. Full-waveform inversion of plane-wave seismograms in stratified acoustic media: Theory and feasibility. Geophysics, 53: 21-31.

Pica, A., Diet, J.P. and Tarantola, A., 1990. Nonlinear inversion of seismic reflection data in a laterally invariant medium. Geophysics, 55(3): 284-292.

Schwab, F.A. and Knopoff, L., 1972. Fast Surface waves and free mode computations. Meth. Comput. Physics, 11: 87-180.

Stoffa, P.L. and Sen, M.K., 1992. Seismic waveform inversion using global optimization. J. Seismic Explor., 1: 9-27.

Thomsen, L., 2002. Understanding Seismic Anisotropy in Exploration and Exploitation. SEG Distinguished Instructor Series, no. 5.

Tiwari, U.K. and McMechan, G.A., 2007a. Effects of incomplete parameterization on inversion of full wavefield viscoelastic seismic data for petrophysical reservoir properties. Geophysics, 72: 09-17.

Tiwari, U.K. and McMechan, G.A., 2007b. Estimation of effective pressure and water saturation by viscoelastic inversion of synthetic time-lapse seismic data for a gas sandstone reservoir. J. Seismic Explor., 16: 57-68.

Xu, T., McMechan, G.A. and Sun, R., 1995. 3-D prestack full-wavefield inversion. Geophysics, 60: 1805-1818.